Korean J. of Chem. Eng., **10**(3), 169-181 (1993)

DYNAMIC GROWTH OF A SPHERICAL BUBBLE IN A TIME-PERIODIC ELECTRIC FIELD

Jin Chan Bae and In Seok Kang*

Department of Chemical Engineering and Advanced Fluids Engineering Research Center,
Pohang Institute of Science and Technology, Pohang 790-600, Korea
(Received 1 April 1993 • accepted 15 July 1993)

Abstract—The dynamics of a spherical bubble in a time-dependent electric field is investigated via the modified Rayleigh-Plesset equation where the effect of an electric field is added. The effect of an imposed electric field is found to be equivalent to the increase of the ambient pressure by the amount of $3/8\varepsilon_0\varepsilon_1 E_0^2(2S-1)$, where $\varepsilon_0\varepsilon_1$ is the electric permittivity of the gas inside the bubble, E_0 the strength of the imposed electric field, S the permittivity ratio of the outside fluid to the inside gas. The effects of a time-periodic electric field have been studied by using two methods of analysis; the two-timing perturbation analysis for the regular dynamics near the stable steady solution and the Poincaré map analysis for the global dynamics. It is revealed that an $O(\varepsilon^{1/3})$ response in the oscillation of bubble radius can be obtained from an $O(\varepsilon)$ resonant time-periodic forcing in the neighborhood of a stable steady solution. By the Poincaré map analysis, it is also shown that the bubble can either undergo bounded oscillation, or else respond chaotically and grow very rapidly. The probability of escape to rapid growth is found to be a strong function of the forcing frequency, of which the optimal value is slightly lower than the intrinsic resonant frequency of oscillation under the steady electric field.

INTRODUCTION

When the local pressure in a fluid falls below the vapor pressure, gas pockets may form and grow. This phenomenon is called cavitation. The pocket may be filled with gases, which have been dissolved or trapped in the fluid, and vapors of the fluid itself. The onset of cavitation depends on many factors such as the size of nucleus, ambient pressure, amount of dissolved gas, vapor pressure, viscosity, surface tension, etc. The driving force for growth or collapse of cavitation bubbles is the pressure difference between the bubble interior and the ambient fluid medium.

The problem of bubble growth associated with cavitation has broad banded application in numerous areas. Familiar examples in chemical engineering include the foaming process and the nucleate boiling process. In the researches for hydromachinery, major concerns have been given to the sound generation by cavitation bubbles that undergo time-dependent change of volume. The damage to the blade surface caused by succesive collapse of cavitation bubbles has been another important concern in that area. An ultra-sonic wave as a form of energy has been used in various applications that are associated with cavitation. Rupture or fragmentation of suspended particles, emulsification of liquid mixtures, and dispersion of small particles are familiar examples. Recently, more exotic applications have been reported. The phenomenon of cavitation induced by an ultrasonic wave is used to increase the chemical reactivities and to improve the microstructure in solidification process [1].

On the other hand, there are many processes where cavitation is not wanted. Erosion and corrosion induced by cavitation are among the typical examples. In those cases, cavitation should be suppressed effectively. One of the suppression methods is to increase the ambient pressure. As an alternative, application of electric field has been considered [2] and the present work is also about the alternative method. An imposed electric field exerts an extra surface force to the bubble surface and has an effect that is equivalent to the increase of the ambient pressure. For a given pressure difference, a *steady* electric field may suppress the formation and the growth of bubbles, which would grow rapidly in the absence of an electric field.

The literature on the bubble dynamics is very exten-

*To whom all correspondences should be addressed.

sive, but earlier works are fairly well summarized in the review article by Plesset and Prosperetti [3]. Thus, only the works that are directly related to the present work are discussed here. The problem of cavitation was first considered by Lord Rayleigh [4]. Later Plesset extended Rayleigh's theory to set up the governing equation for the cavitation problem, which is now known as the Rayleigh-Plesset equation (see the reference [3]). Recently Chang and Chen [5] applied the theory of nonlinear dynamics to the Rayleigh-Plesset equation to predict the condition for cavitation under steady ambient pressure field. The work of Chang and Chen was further extended by Szeri and Leal [6] to include the effect of time-dependent pressure field. However, their analysis was intended mainly to estimate the condition of cavitation and the dynamics of a bubble under time-periodic pressure field was not discussed in detail.

In the present work, we are concerned with the effects of an electric field on the bubble dynamics. We are interested primarily in the dynamical responses of a bubble in a time-periodic electric field. As discussed in the above, imposing an electric field is equivalent to the increase of the ambient pressure if the sphericity of bubble shape is assumed. Thus, an electric field can be considered as an alternative tool for controlling the ambient pressure field. That is the case especially when the pressure control is difficult. In the qualitative and mathematical senses, the present problem is very much similar to the problem of bubble dynamics in time-periodic straining flows. Thus, we follow very closely the work of Kang and Leal [7], who analyzed the effects of a time-periodic straining flow by using the Poincaré map analysis. As will be shown later, the Poincaré map analysis will prove to be an effective tool for understanding the complicated dynamical behaviors of a bubble in a time-periodic electric field. Furthermore, the analysis will show that a time-periodic electric field may be used to promote cavitation in a fluid, although a steady electric field is mainly employed to inhibit the cavitation.

DERIVATION OF DYNAMICAL EQUATION

We consider a spherical bubble in a quiescent fluid which is undergoing growth or collapse in the presence of a time-dependent electric field $\mathbf{E}_0(t)$ as shown in Fig. 1. The interior and exterior of the bubble are indicated by '1' and '2' respectively. The bubble interior is composed of some permanent gas and the vapor of the surrounding fluid at constant temperature. The fluids in both sides of the bubble are assumed to possess uniform and isotropic material properties, such as viscosity(μ), density(ρ), electric conductivity(σ) and relative permittivity(ε). For convenience, we define the ratios of the material properties as

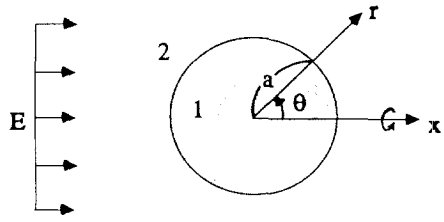

Fig. 1. A spherical bubble in a quiescent fluid in the presence of a time-dependent electric field.

$$R\equiv\frac{\sigma_1}{\sigma_2},\ S\equiv\frac{\varepsilon_2}{\varepsilon_1},\ M\equiv\frac{\mu_2}{\mu_1}. \tag{1}$$

For common fluids, R, S, and M are not zero and have finite values. For the case of bubble, $R\ll 1$ and $S,\ M\geq 1$, since the fluid inside the bubble is nearly nonconducting and inviscid. We also assume that the surface of bubble is characterized by a uniform surface tension γ. The distributions of electric field inside and outside the bubble can be obtained via the electric field potential that is defined as $\mathbf{E}=-\nabla\psi$. When the free charge is absent within the fluid media and the permittivities are uniform, the governing equations for the electric potentials are

$$\nabla^2\psi_1=0,\ \nabla^2\psi_2=0. \tag{2}$$

The corresponding boundary conditions are [8]:

B.C.1 The field be finite at the origin ($r=0$).

B.C.2 Tangential component of the electric field be continuous at the interface, i.e. $\mathbf{n}\times[\mathbf{E}]=0$. Hence,

$$\frac{\partial\psi_1}{\partial s}=\frac{\partial\psi_2}{\partial s}\ \text{at}\ r=a \tag{3}$$

where a is the radius of bubble and s is the arclength along the bubble surface.

B.C.3 Conduction current normal to the interface be continuous, i.e. $\mathbf{n}\cdot[\mathbf{J}]=0$, where $\mathbf{J}=\sigma\mathbf{E}$ for ohmic fluids. Hence

$$\sigma_1\frac{\partial\psi_1}{\partial n}=\sigma_2\frac{\partial\psi_2}{\partial n}\ \text{at}\ r=a \tag{4}$$

where derivatives are evaluated in the direction of the outward normal vector $\mathbf{n}$.

B.C.4 Electric field at infinity is unidirectional, i.e. $\mathbf{E}_2\rightarrow E_0(t)\mathbf{e}_x$ as $r\rightarrow\infty$. Hence

$$\nabla\psi_2 \rightarrow -E_0(t)\mathbf{e}_x \text{ as } r\rightarrow\infty \tag{5}$$

where $E_0(t)$ is the magnitude of electric field at infinity.

One comment should be given here to the boundary condition (4). In the case of no free surface charge, the normal component of electric displacement must be continuous across the boundary, i.e.

$$\varepsilon_1\frac{\partial\psi_1}{\partial n}=\varepsilon_2\frac{\partial\psi_2}{\partial n} \text{ at } r=a. \tag{6}$$

Thus, we can see from (4) and (6) that $\sigma_1/\sigma_2=\varepsilon_1/\varepsilon_2$, i.e. $RS=1$ in that case (see pp. 216-217 of the book by Nafeh and Brussel [9]).

Since the bubble shape is assumed to be spherical, it is convenient to solve the problem using the spherical coordinate system, with the axis of symmetry corresponding to $\theta=0$ and $\theta=\pi$ as shown in Fig. 1. The solutions for the electric potentials are easily obtained by the method of eigenfunction expansion as (see Melcher and Taylor [8])

$$\begin{aligned}
E_{r1}&=-\frac{\partial\psi_1}{\partial r}=E_0\left(\frac{3}{R+2}\right)\cos\theta,\\
E_{\theta 1}&=-\frac{1}{r}\frac{\partial\psi_1}{\partial\theta}=-E_0\left(\frac{3}{R+2}\right)\sin\theta,\\
E_{r2}&=-\frac{\partial\psi_2}{\partial r}=E_0\left[1-\left(\frac{1-R}{R+2}\right)\frac{2a^3}{r^3}\right]\cos\theta,\\
E_{\theta 2}&=-\frac{1}{r}\frac{\partial\psi_2}{\partial\theta}=-E_0\left[1+\left(\frac{1-R}{R+2}\right)\frac{a^3}{r^3}\right]\sin\theta.
\end{aligned} \tag{7}$$

In the above, it is worthy of note that the electric field inside the bubble is uniform, i.e.

$$\mathbf{E}_i=\frac{3}{R+2}E_0(t)\mathbf{e}_x.$$

The stress resulted from the electric field can be evaluated by using the Maxwell stress tensor defined as

$$\mathbf{T}=\varepsilon_0\varepsilon\mathbf{E}\mathbf{E}-\frac{1}{2}\varepsilon_0\varepsilon E^2\mathbf{I}. \tag{8}$$

where ε_0 is the permittivity in vacuum. Thus the electrical surface force density on a spherical surface is obtained as

$$\begin{aligned}
\mathbf{t}_n^e&=\mathbf{n}\cdot\mathbf{T}^e=\mathbf{n}\cdot\mathbf{T}_2^e-\mathbf{n}\cdot\mathbf{T}_1^e\\
&=(T_{r2}^e-T_{r1}^e)\mathbf{e}_r+(T_{r\theta 2}^e-T_{r\theta 1}^e)\mathbf{e}_\theta\\
&=t_n\mathbf{e}_r+t_s\mathbf{e}_\theta.
\end{aligned} \tag{9}$$

where t_n and t_s are the normal and tangential components of the surface force density. From (8) T_{rr}^e and $T_{r\theta}^e$ are expressed as

$$\begin{aligned}
T_{rr}^e&=\frac{1}{2}\varepsilon_0\varepsilon(E_r^2-E_\theta^2),\\
T_{r\theta}^e&=\varepsilon_0\varepsilon E_rE_\theta.
\end{aligned} \tag{10}$$

Then we can obtain t_n and t_s at the bubble surface as

$$\begin{aligned}
t_n&=\frac{9}{2}\varepsilon_0E_0^2\frac{\varepsilon_1}{(R+2)^2}[\{S(R^2+1)-2\}\cos^2\theta+(1-S)],\\
t_s&=9\varepsilon_0E_0^2\varepsilon_1\frac{(1-RS)}{(R+2)^2}\cos\theta\sin\theta.
\end{aligned} \tag{11}$$

As we can see above, the normal stress is not uniform along the bubble surface. Thus, the bubble would deform into a spheroidal shape if the surface tension is not sufficiently strong. Here, however, for simplicity in analysis we take a critical assumption that the shape of the bubble remains spherical during the whole process of growth and collapse. To obtain the effects of electric field under the assumption of spherical shape, we take averages of the normal and tangential contributions of the electrical surface force over the entire surface to have

$$\begin{aligned}
\langle t_n\rangle&=\frac{1}{A}\int t_n(\theta)dA\\
&=\frac{9}{2}\varepsilon_0E_0^2\varepsilon_1\frac{1}{(R+2)^2}\left[\frac{1}{3}\{S(R^2+1)-2\}+(1-S)\right],\\
\langle t_s\rangle&=\frac{1}{A}\int t_s(\theta)dA=0.
\end{aligned} \tag{12}$$

For the case of a bubble in which $R\ll 1$, $\langle t_n\rangle$ reduces to

$$\langle t_n\rangle=-\frac{3}{8}\varepsilon_0E_0^2\varepsilon_1(2S-1). \tag{13}$$

Therefore the electric field exerts a suppressive force on the bubble surface since $\langle t_n\rangle$ is negative for usual bubbles ($S\gg 1$). In (12) and (13), it is noteworthy that $\langle t_n\rangle$ is independent of the bubble radius and the relations hold even for the limit $a\rightarrow 0$.

Now, we consider the motion of the interface induced by changes in the volume of a single spherical bubble that is suspended in an incompressible and Newtonian fluid in the presence of an uniform electric field. In order to predict the bubble radius as a function of time in the presence of a prescribed ambient pressure field and an electric field, we begin with the Rayleigh-Plesset equation (for derivation of this famous equation, see the book by Leal [10])

$$\begin{aligned}
a\ddot{a}+\frac{3}{2}\dot{a}^2=\frac{1}{\rho}&[p_v(T_\infty)+p_g(t)-p_\infty(t)]\\
&-\frac{1}{\rho}\left[\frac{2\gamma}{a}+\frac{4\mu_2\dot{a}}{a}\right]
\end{aligned} \tag{14}$$

where p_v, p_g, p_∞ are the vapor pressure of the ambient fluid at the bubble temperature, the pressure contribution of the permanent gas, and the ambient pressure, respectively. In general, thermal effect plays an important role on the dynamics of a gas/vapor bubble. However, we restrict our concern only to the isothermal cases and use the ideal gas law for the convenience in analysis. The contribution due to the permanent gas can then be represented as

$$p_g(t)=\frac{GT_\infty}{a^3}=\frac{\hat{G}}{a^3},$$

where G and $\hat{G}$ are appropriate constants. Thus, we have

$$a\ddot{a}+\frac{3}{2}\dot{a}^2=\frac{1}{\rho}[p_v-p_\infty(t)]+\frac{1}{\rho}\left[\frac{\hat{G}}{a^3}-\frac{2\gamma}{a}-\frac{4\mu_\infty\dot{a}}{a}\right]. \quad (15)$$

As we have seen in (12), the electric field has an effect of increasing the ambient pressure by $-\langle t_n\rangle$ and we thus have the modified Rayleigh-Plesset equation as

$$a\ddot{a}+\frac{3}{2}\dot{a}^2=\frac{1}{\rho}[p_v-p_\infty(t)]+\frac{1}{\rho}\left[\frac{\hat{G}}{a^3}-\frac{2\gamma}{a}-\frac{4\mu_\infty\dot{a}}{a}\right]+\frac{9\varepsilon_0E_0^2\varepsilon_1}{2\rho(R+2)^2}\left[\frac{1}{3}\{S(R^2+1)-2\}+(1-S)\right]. \quad (16)$$

For the case of a bubble in which $R\ll 1$,

$$a\ddot{a}+\frac{3}{2}\dot{a}^2=\frac{1}{\rho}[p_v-p_\infty(t)]+\frac{1}{\rho}\left[\frac{\hat{G}}{a^3}-\frac{2\gamma}{a}-\frac{4\mu_\infty\dot{a}}{a}\right]-\frac{3\varepsilon_0E_0^2\varepsilon_1}{8\rho}(2S-1). \quad (17)$$

Now, let us nondimensionalize the modified Rayleigh-Plesset equation, where the effect of an electric field is included. We may choose one specific ambient pressure $\hat{p}_\infty$ as the characteristic pressure scale. But the problem here is that we do not have an explicit length scale for this problem because the bubble radius itself is a dependent variable. Thus, we choose one of the equilibrium radii, $\hat{a}_E$, for the given ambient pressure $p_\infty=\hat{p}_\infty$ as the characteristic length scale. When a steady electric field is present and $R\ll 1$, the equilibrium radius can be obtained from

$$\frac{1}{\rho}\left[p_v-\hat{p}_\infty-\frac{3}{8}\varepsilon_0E_0^2\varepsilon_1(2S-1)\right]+\frac{1}{\rho}\left[\frac{\hat{G}}{\hat{a}_E^3}-\frac{2\gamma}{\hat{a}_E}\right]=0 \quad (18)$$

As will be shown later, (18) has either zero, one or two physically meaningful (positive) solutions depending on the parameters. Thus, $\hat{p}_\infty$ must be an ambient pressure that ensures the existence of a positive solution, and we choose the smaller radius as our characteristic scale in the case of two positive solutions. The nondimensionalized equation with the characteristic scales

$$l_c=\hat{a}_E,\ p_c=\hat{p}_\infty,\ t_c=\left(\frac{\rho\hat{a}_E^3}{\gamma}\right)^{1/2},$$

is then

$$\tilde{a}\ddot{\tilde{a}}+\frac{3}{2}\dot{\tilde{a}}^2+\frac{4}{Re}\frac{\dot{\tilde{a}}}{\tilde{a}}=B\Delta P(t)-\frac{3}{8}W(t)\varepsilon_1(2S-1)+\frac{MB}{\tilde{a}^3}-\frac{2}{\tilde{a}} \quad (19)$$

where $\tilde{a}=a/\hat{a}_E$ and the dimensionless parameters are

$$Re\equiv\frac{\rho\hat{a}_E^2}{\mu t_c}=\frac{(\rho\hat{a}_E\gamma)^{1/2}}{\mu},$$

$$B\equiv\frac{\hat{p}_\infty a_E}{\gamma}=\frac{\text{pressure force}}{\text{surface tension force}},$$

$$M\equiv\frac{\hat{G}}{\hat{p}_\infty\hat{a}_E^3},\ \Delta P(t)=\frac{p_v-p_\infty}{\hat{p}_\infty},$$

$$W(t)\equiv\frac{\varepsilon_0E_0(t)^2\hat{a}_E}{\gamma}=\frac{\text{electric force}}{\text{surface tension force}}.$$

In the above, $W(t)$ is termed the (electrical) Weber number in the sense that the number represents the ratio of the deforming electrical force to the restoring surface tension force.

At this point, it is appropriate to estimate the values of the timescale, t_c, and the damping coefficient, $1/Re$, for the cavitation bubbles in aqueous solution. For simplicity, if we assume $\gamma=O(100)$ dyne/cm, then $t_c=10^{-1}$ sec, 10^{-4} sec, and 10^{-7} sec and $1/Re=10^{-3}$, 10^{-2}, and 10^{-1} for $\hat{a}_E=1$ cm, 10^{-2} cm, 10^{-4} cm respectively. Thus, we can see that if the bubble radius is smaller than $O(10^{-3})$cm, then $t_c<O(10^{-5})$sec. Thus, the characteristic timescale is in the range of ultrasonic wave (ultrasonic wave has the frequency over $O(2\times10^4)$Hz).

STEADY SOLUTIONS

Now we consider the equilibrium solution of (19) for the case of steady pressure difference ($\Delta P=$*constant*) and steady electric field [$W(t)=W=$*constant*]. In that case, (19) reduces to

$$\Delta P-\frac{3}{8}\frac{W}{B}\varepsilon_1(2S-1)=\frac{2}{B}\frac{1}{\tilde{a}_E}-\frac{M}{\tilde{a}_E^3}. \quad (20)$$

In Fig. 2, plots of ΔP versus $\tilde{a}_E$ are shown for several Weber numbers in the case of $B=0.5$, $M=1$, $S=100$, and $\varepsilon_1=1$. As we can see in (20) and Fig. 2, the effect of an imposed electric field is merely a shift of the

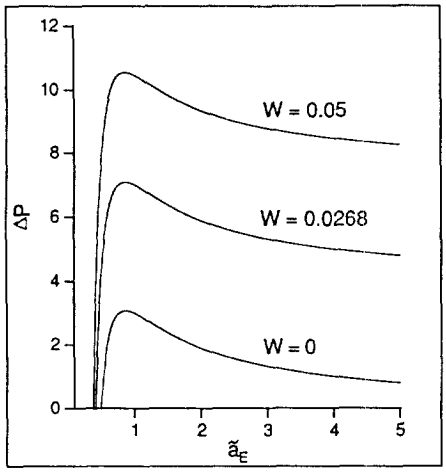

Fig. 2. Equilibrium radius $\tilde{a}_E$ as an inverse function of the pressure difference when the Weber number $W=0$, $W=0.0268$ and $W=0.05$.

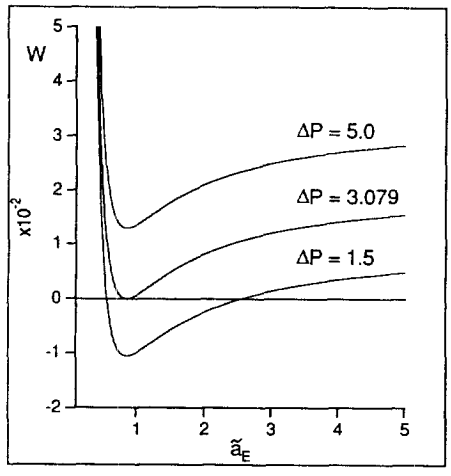

Fig. 3. Equilibrium radius $\tilde{a}_E$ as an inverse function of the Weber number for various values of the pressure difference.

plot by the amount of (3/8) $(W/B)\varepsilon_1(2S-1)$ in the direction of ΔP axis. From Fig. 2, we see also that Eq. (20) has no positive solution if ΔP exceeds a certain value ΔP_{cri}. Physically, it means that if $\Delta P>\Delta P_{cri}$ a bubble grows indefinitely, i.e. cavitation occurs. Thus, it is important to estimate that value. To do that, we get the critical radius $\tilde{a}_{cri}$ where ΔP has the maximum value. The results are

$$\tilde{a}_{cri}=\sqrt{\frac{3BM}{2}},\quad \Delta P_{cri}=\sqrt{\frac{32}{27B^3M}}+\frac{3}{8}\frac{W}{B}\varepsilon_1(2S-1). \tag{21}$$

By substituting the definitions of the dimensionless parameters, we can represent the results (21) in dimensional form as

$$a_{cri}=\sqrt{\frac{3\hat{G}}{2\gamma}},\quad \Delta p_{cri}=\sqrt{\frac{32\gamma^3}{27\hat{G}}}+\frac{3}{8}\varepsilon_0E_0^2\varepsilon_1(2S-1) \tag{22}$$

From Fig. 2, we can see that when $\Delta P<\Delta P_{cri}$, two equilibrium radii are possible if

$$\frac{3}{8}\frac{W}{B}\varepsilon_1(2S-1)<\Delta P<\Delta P_{cri},$$

and only one equilibrium radius is possible if

$$\Delta P<\frac{3}{8}\frac{W}{B}\varepsilon_1(2S-1).$$

For the case of two equilibrium solutions, as will be shown shortly in next section, only one of two solutions is stable. If the equilibrium radius is larger than $\tilde{a}_{cri}$, i.e.

$$\tilde{a}_E>\tilde{a}_{cri}$$

than $\tilde{a}_E$ is unstable and physically not attainable.

There are limiting values of W for existence of steady state solution for fixed values of ΔP. Fig. 3 shows W versus $\tilde{a}_E$ plots for case of $B=0.5$, $M=1.0$, $S=100$ and $\varepsilon_1=1.0$. As we can see in Fig. 3, if $\Delta P>3.079$, there are critical Weber numbers W_{c1} and W_{c2} for existence of steady solutions. The number of steady solutions is 0 if $W<W_{c1}$, 2 if $W_{c1}<W<W_{c2}$, and 1 if $W>W_{c2}$.

At this point, it would be appropriate to discuss in more detail the case of permanent gas. In this case, $\hat{G}=0$ (and so $M=0$), and (20) has only one solution

$$\tilde{a}_E=\frac{2}{B\Delta P-(3/8)W\varepsilon_1(2S-1)}. \tag{23}$$

This solution is unstable in the sense that the bubble grows if $\tilde{a}>\tilde{a}_E$, but shrinks if $\tilde{a}<\tilde{a}_E$. Thus, the equilibrium radius of (23) is called the critical radius fo the homogeneous nucleation of vapor phase. Since $S=\varepsilon_2/\varepsilon_1$, (23) reduces to

$$\tilde{a}_E=\frac{2}{B\Delta P-(3/4)W\varepsilon_2}. \tag{24}$$

when $S\gg1$. As we can see in (24), the imposed *steady* electric field makes the critical radius larger and thus inhibits homogeneous nucleation. The result (24) was obtained earlier by Marston and Apfel [2].

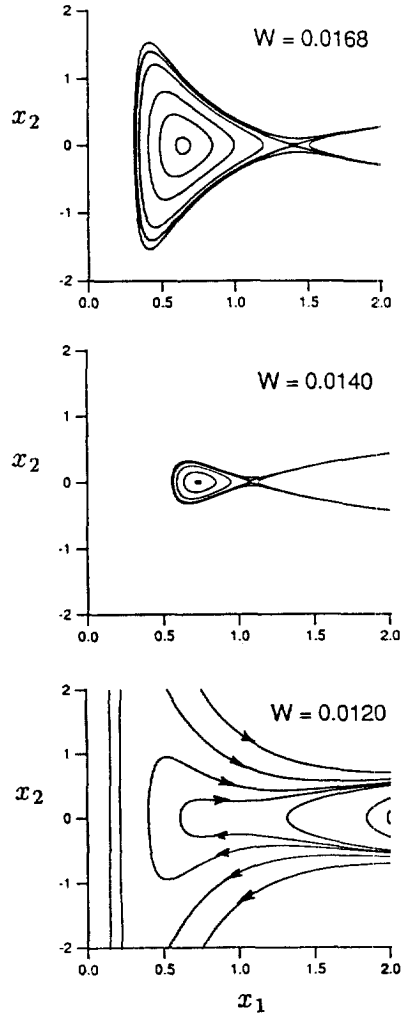

Fig. 4. Phase-plane portraits for the dynamics of a bubble in a steady electric field when $\Delta P=5$, $B=0.5$, $M=1$, $S=100$, $\varepsilon_1=1$ and there is no viscous damping.

DYNAMICS

1. Dynamics of a bubble in a steady electric field

Now we consider the full dynamics of the Rayleigh-Plesset equation in terms of the nonlinear dynamics. Let us begin with the case of steady electric field [$W(t)=W=constant$]. By defining $x_1\equiv\bar{a}$ and $x_2=\dot{x}_1=\dot{\bar{a}}$, a system of equations is obtained from the Rayleigh-Plesset equation in dimensionless form as

$$\dot{x}_1=x_2\equiv f_1(x_1,\ x_2)$$

$$\dot{x}_2=-\frac{3}{2}\frac{x_2^2}{x_1}-\frac{4}{Re}\frac{x_2}{x_1^2}+B\Delta P\frac{1}{x_1}-\frac{3}{8}W\varepsilon_1(2S-1)\frac{1}{x_1}$$

$$-\frac{2}{x_1^2}+\frac{MB}{x_1^4}\equiv f_2(x_1,\ x_2). \tag{25}$$

The best way to study the dynamical systems such as one given in (25) is to use phase-plane portraits. In Fig. 4, there are three phase-plane portraits for the case of no viscous damping ($1/Re=0$) and $\Delta P=5$. In the cases of $W=0.014$ and 0.0168, there exist two steady solutions, but no steady solution exists when $W=0.012$. Remind the fact that there exist two equilibrium solutions when $W_{c1}<W<W_{c2}$. In the case of $W=0.0168$, the $(x_1,\ x_2)$ phase space has two equilibria at (0.65, 0) and (1.4, 0). As well known, each contour in the phase-plane portraits of the Hamitonian case represents the equi-energy line. Thus, the equilibrium solution at (0.65, 0) has a local minimum energy and corresponds to a center or elliptic point, while the equilibrium solution at (1.4, 0) corresponds to a saddle point in the energy distribution and is unstable. One more thing we should note from Fig. 4 is that there exists a separatrix which starts from and end at the saddle point and encircles the stable equilibrium solution. Therefore the bubble may grow very rapidly even in the case of $W_{c1}<W<W_{c2}$, if the initial condition is outside the separatrix. This behavior cannot be predicted by any linear theory and is certainly due to the nonlinear effect.

Before going on to the dynamic response to a time-periodic forcing of the electric field, let us discuss the effect of electric field on the natural frequency of oscillation about the stable equilibrium solution. We define deviation variables, $y_1=x_1-x_{1s}$, $y_2=x_2-x_{2s}$ where x_{1s} and x_{2s} are the stable steady state solutions. From the linear stability analysis, we may obtain the frequency of oscillation as a function of x_{1s},

$$\omega_0^2=\frac{3MB}{x_{1s}^5}-\frac{2}{x_{1s}^3}, \tag{26}$$

where ω_0 is the natural frequency of oscillation. The dependency of natural frequency on the electrical Weber number is shown in Fig. 5 in the case of $B=0.5$, $M=1.0$, $S=100$, $\varepsilon_1=1.0$. We can see that the natural frequency of oscillation increases as the Weber number increases. Since the increase of the Weber number is equivalent to the decrease of the pressure difference, the frequency of oscillation increases as the pressure difference decreases. As we can see from Figs. 2 and 3, the stable equilibrium radius decreases as the Weber number increases or the pressure difference decreases. Since the smaller bubble oscillates faster than the larger one, the frequency increases with the increase of W. One more thing we can note from (26) is that the oscillation frequency becomes

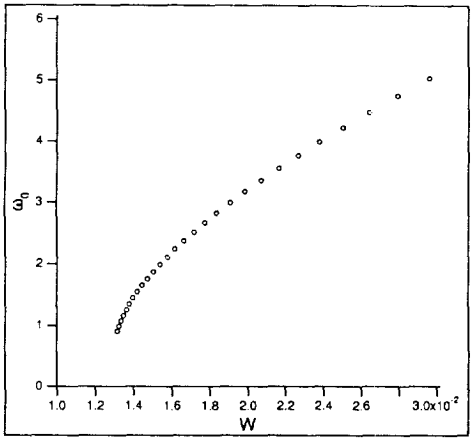

Fig. 5. The natural frequency as a function of the Weber number (other parameters are the same as in Fig. 4).

exactly zero at the critical radius. This can be easily verified by Eqs. (21) and (26).

2. Regular dynamics of a bubble in a time-periodic electric field

As we have seen in Fig. 4, for the case of steady electric field with no viscous damping, the dynamical system (25) is a Hamiltonian system with a saddle point and a center. Now we are interested in the dynamical behaviors of a bubble subject to a time-dependent electric field. We consider first the case of a time-periodic electric field which is given as

$$E(t)=E_0(1\pm\varepsilon\cos\omega t).$$

Then the Weber number is

$$W(t)=W_0(1\pm\varepsilon\cos\omega t)^2=W_0(1\pm 2\varepsilon\cos\omega t)+O(\varepsilon^2).$$

The behaviors of a dynamical system with time-periodic forcing can be best investigated via the Poincaré map analysis. In fact the Poincaré map is nothing but a phase-plane portrait for which the data are taken only for the times that are multiples of given forcing period (see references such as Guckenheimer and Holmes [11]). Thus, for a Hamiltonian system with a steady forcing, the Poincaré map and the usual phase-plane portrait are identical. The question now is what kind of change is expected in the Poincaré map for the case of time-periodic forcing. Near the elliptic point, almost all of the closed orbitals on the Poincaré map are preserved when ε is small due to the Kolmogorov-Arnold-Moser (KAM) theorem (see Guckenheimer and Holmes). Therefore we consider first the regular dynamical response, in the sense that the dynamics can be studied analytically, to the small amplitude oscillation of the electric field with the assumption that the deviation of the bubble radius from a_E is small. Then the system (25) is changed to give

$$\dot{x}=x_2\equiv f_1(x_1,\ x_2)$$

$$\dot{x}_2=-\frac{3}{2}\frac{x_2^2}{x_1}+B\Delta P\frac{1}{x_1}-\frac{3}{8}W_0\varepsilon_1(2S-1)\frac{1}{x_1}-\frac{2}{x_1^2}+\frac{MB}{x_1^4}\mp\varepsilon\frac{3}{4}W_0\varepsilon_1(2S-1)\frac{1}{x_1}\cos\omega t\equiv f_2(x_1,\ x_2). \tag{27}$$

In terms of disturbance variables y_1, y_2 defined earlier, (27) is expanded up to $O(y_1^2)$, $O(y_1y_2)$, $O(y_2^2)$ and to the order of $O(\varepsilon)$. Then,

$$\dot{y}_1=y_2$$
$$\dot{y}_2=-\omega_0^2y_1+Cy_1^2+Dy_2^2\mp\varepsilon FW_0\cos\omega t. \tag{28}$$

where ω_0 is the intrinsic frequency of oscillation for the case of $W=W_0$ which was mentioned earlier and

$$C=\frac{B\Delta P}{x_{1s}^3}+\frac{10MB}{x_{1s}^6}-\frac{6}{x_{1s}^4}-\frac{3}{8}W_0\varepsilon_1(2S-1)\frac{1}{x_{1s}^3}$$
$$D=-\frac{3}{2}\frac{1}{x_{1s}},\quad F=\frac{3}{4x_{1s}}\varepsilon_1(2S-1).$$

By defining $u=y_1$ and $\dot{u}=y_2$ for convenience, (28) can be represented as

$$\ddot{u}+\omega_0^2u-Cu^2-D\dot{u}^2=\mp\varepsilon(FW_0)\cos\omega t. \tag{29}$$

The dynamical natures of (29) has been thoroughly studied previously by Kang and Leal [7] and Kang [12] for the analysis of similar problems in the bubble and drop dynamics. Thus, here we touch the equation very briefly.

The above dynamic equation for an inviscid bubble near the stable steady state is now investigated up to the square terms in resonant cases. We define $\tilde{\varepsilon}\equiv\varepsilon(FW_0)$ and consider the resonant case where $\omega=\omega_0$. Then (29) becomes

$$\ddot{u}+\omega_0^2u-Cu^2-D\dot{u}^2=\mp\tilde{\varepsilon}\cos\omega t. \tag{30}$$

The response of a nonlinear oscillator to a weak periodic forcing at a resonant frequency is often characterized by multiple time scales. As shown by Kang and Leal [7] and Kang [12], the resonant response of the above dynamical equation for small $\tilde{\varepsilon}$ is $O(\tilde{\varepsilon}^{1/3})$ and exhibits two-timing behaviors. Therefore a slow periodic oscillation (which has a long-time-scale variable τ) is superposed on a higher frequency oscillation that is near the forcing frequency. In this case, the analysis for the resonant response requires the so-called two-timing or two-variable expansion procedure, i.e.

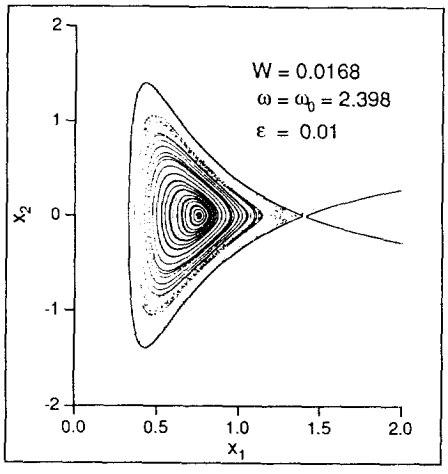

Fig. 6. The Poincaré map for the case of exact resonant forcing ($\omega=\omega_0=2.398$) when $\varepsilon=0.01$, $W_0=0.0168$ (other parameters are the same as in Fig. 4).

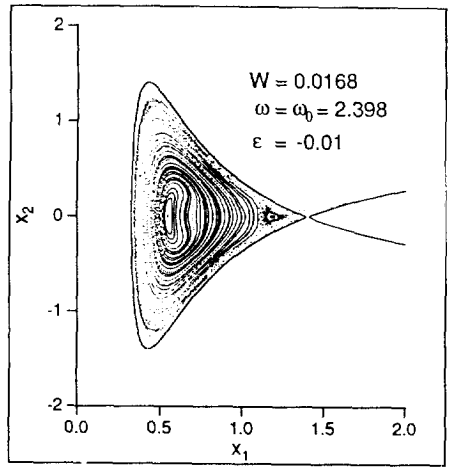

Fig. 7. The Poincaré map for the case of exact resonant forcing ($\omega=\omega_0=2.398$) when $\varepsilon=-0.01$, $W_0=0.0168$ (other parameters are the same as in Fig. 4).

$$\tau=\tilde{\varepsilon}^{2/3}t,$$
$$u(t,\tau)=\sum_n \tilde{\varepsilon}^{n/3}g_n(t,\tau). \tag{31}$$

The scalings in (31) can be found without difficulty (Any interested reader may consult the book by Nafeh and Mook [13]). The $O(\tilde{\varepsilon}^{1/3})$ solution is found to be

$$u(t,\tau)\sim\tilde{\varepsilon}^{1/3}A(\tau)\cos[\omega t-\phi(\tau)] \tag{32}$$

where $A(\tau)$ and $\phi(\tau)$ satisfy a system of equations

$$\frac{dA}{d\tau}=\mp\frac{1}{2\omega}\sin\phi,$$
$$A\frac{d\phi}{d\tau}=\frac{(5C^2+5CD\omega^2+2D^2\omega^4)A^3}{12\omega^3}\mp\frac{\cos\phi}{2\omega}. \tag{33}$$

The significance of (32) is that the nonlinearities in the system amplifies $O(\tilde{\varepsilon})$ resonant forcing to produce $O(\tilde{\varepsilon}^{1/3})$ output. The fixed points, where both ϕ and A are time-independent are found to be (A^*, π) for $\tilde{\varepsilon}\cos\omega t$ forcing and $(A^*, 0)$ for $-\tilde{\varepsilon}\cos\omega t$ forcing, where

$$A^*=\left[\frac{6\omega^2}{(5C^2+5CD\omega^2+2D^2\omega^4)}\right]^{1/4}. \tag{34}$$

At the fixed points, both A and ϕ are time-independent and a bubble undergoes oscillation with a fixed amplitude and a phase shift as we can see in (32).

The two-timing solution may be transformed to the Poincaré map directly by substituting $t=nT$, where T is the period of forcing, i.e., $T=2\pi/\omega$. Then, in terms of x_1 and x_2 the Poincaré map is obtained as

$$x_1(nT)=u(nT)+x_{1s}\sim\tilde{\varepsilon}^{1/3}A(\tau_n)\cos(\phi(\tau_n))+x_{1s}$$

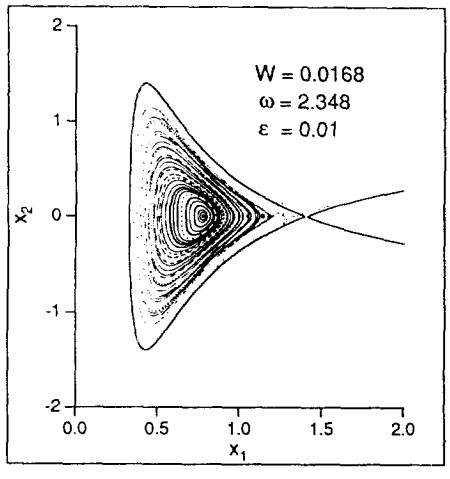

Fig. 8. The Poincaré map for the case of nearly resonant forcing ($\omega=2.348$) when $\varepsilon=0.01$, $W_0=0.0168$.

$$x_2(nT)=\dot{u}(nT)\sim\tilde{\varepsilon}^{1/3}\omega A(\tau_n)\sin(\phi(\tau_n)) \tag{35}$$

where $\tau_n\equiv\tilde{\varepsilon}^{2/3}(nT)$. We can see that the fixed point in the Poincaré map has shifted from elliptic point by $(-A^*, 0)$ for $\tilde{\varepsilon}\cos\omega t$ forcing in (30) and $(A^*, 0)$ for $-\tilde{\varepsilon}\cos\omega t$ forcing. In Figs. 6 and 7, the Poincaré maps generated by numerical integration of the full dynamical equation (27) are given. As we can see, the fixed points are shifted by $(A^*, 0)$ for $\varepsilon=0.01$ and $(-A^*, 0)$ for $-\varepsilon=-0.01$ as predicted by the two-timing analysis (note the sign change in the second equation of (27)).

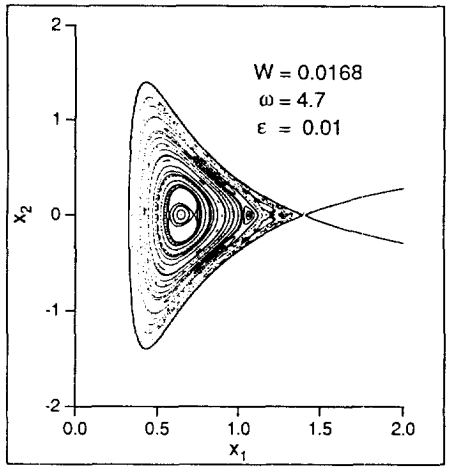

Fig. 9. The Poincaré map for the case of nearly $n=2$ resonant forcing ($\omega=4.7$) when $\varepsilon=0.01$, $W_0=0.0168$.

In Fig. 8, a Poincaré map is given for a nearly resonant case ($\omega=2.348$) which is slightly lower than the intrinsic frequency ω_0 ($=2.398$). By comparing this case with the case of exact resonance in Fig. 6, we can see that the resonance effect is even stronger at a frequency that is slightly lower than the intrinsic frequency ω_0. This phenomenon of stronger resonance at slightly lower frequency than the intrinsic frequency was predicted by the two-timing analysis in Kang [12].

If the forcing frequency is far from ω_0, no interesting results are expected up to the leading order solution, but a multiple timescale response is expected for $\omega\sim n\omega_0$ when we consider higher order solutions. As an example, the Poincaré map for $\omega=4.7\sim2\omega_0$ is presented in Fig. 9.

3. Chaotic dynamics of a bubble and escape to rapid growth

Every trajectory of a dynamic system comes from somewhere and goes somewhere. Very exceptionally, a trajectory comes from a saddle and also goes to another saddle. Such a trajectory is called a saddle connection, or a heteroclinic trajectory. It is even possible for a trajectory to connect a saddle to itself. This trajectory is called a homoclinic trajectory (or a homoclinic orbit) (see references [11, 14] for the terminologies in the theory of nonlinear dynamics). In fact, the phase plane portrait in the present problem possess a homoclinic orbit if $W_{c1}<W<W_{c2}$ (see the phase plane portraits in Fig. 4 which are the same as the corresponding unperturbed Poincaré maps). The dynamical system with a homoclinic or heteroclinic orbit under steady forcing is known to exhibit very complicated

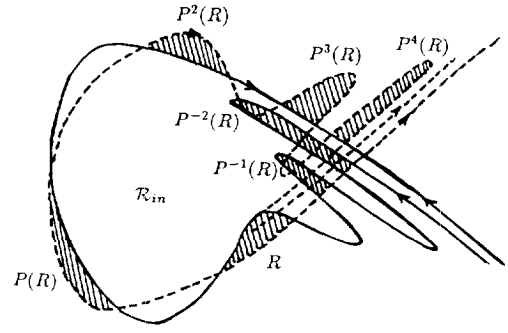

Fig. 10. A schematic representation of the homoclinic tangling phenomena in the Poincaré maps.

behaviors when the system is subject to a time-periodic forcing. The complicated dynamical behaviors have been studied via the concept of homoclinic orbit tangling in the Poincaré maps such as one shown in Fig. 10. The concept of homoclinic orbit tangling is well explained in the references [11, 14]. Any interested reader can consult the references. However, very briefly and roughly, it can be stated that if the initial condition is in the region of homoclinic tangle then the bubble will eventually escape to rapid growth.

For an illustrative purpose, let us define the inside region R_{in} as the region bounded by the stable manifold (solid line) for $x_2\geq0$ and unstable manifold (dotted line) for $x_2<0$ in Fig. 10. If a point is in the region $R\subset R_{in}$ at a certain time, then the point is mapped after each period to the points in the shaded regions according to the sequence

$$R\rightarrow P(R)\rightarrow P^2(R)\rightarrow P^3(R)\rightarrow\cdots.$$

Thus, a point in the tangle region in R_{in} will exhibit apparently random motion for a while and will be pumped to the outside of R_{in} eventually. In Fig. 10, we should note that the region $P^n(R)$ is extended indefinitely as the unstable manifold approaches the saddle point, since the area of each shaded region has the same area for the Hamiltonian case (see Guckenheimer and Holmes [11]). Once the point is pumped out, then both x_1 and x_2 will increase indefinitely.

As we have seen in Fig. 10, the domain of R_{in} can be divided into two parts as $R_{in}=R_{reg}+R_{cha}$, where R_{reg} and R_{cha} denote the regular and chaotic regions and R_{cha} is defined as $R_{cha}=(\cup_{n=0}^{\infty}P^n(R))\cap R_{in}$. Physically, if the initial condition of a bubble is at some point in $R_{cha}\subset R_{in}$, the bubble escapes eventually to the rapid growth stage after several periods. During the several periods of forcing, the bubble will exhibit chaotic oscillation as will be shown later by the plots x_1 vs.

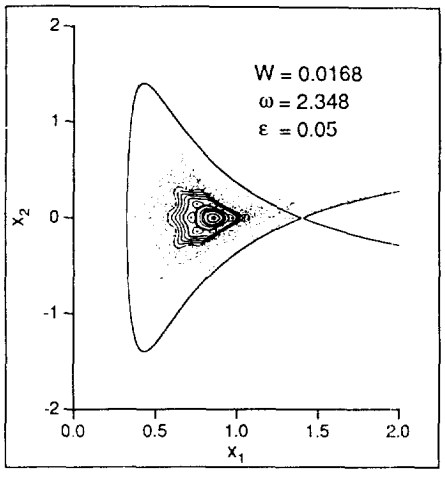

Fig. 11. The Poincaré map for the case of nearly resonant forcing ($\omega=2.348$) when $\varepsilon=0.05$, $W_0=0.0168$.

t. On the other hand, if the initial condition is in R_{no}, the bubble can never escape to the rapid growth stage and it shows bounded oscillation. In fact, the Poincaré maps in Figs. 6-9 were prepared by integrating the governing equations starting from the initial distribution of points along the $x_2=0$ axis. As we can see in the Poincaré maps, there are two regions in R_m; one is quite regular and the other looks random. Thus the size of regular region indicates the region for the initial conditions for bounded oscillation. If the size of the regular region gets smaller then it means the probability of rapid growth gets larger. As discussed above, the homoclinic tangling reduces the size of the region for the bounded oscillation in the phase plane. Thus, the probability of unbounded growth increases as the degree of homoclinic tangling increases.

With a limited but basic understanding on the Poincaré map mentioned above, let us study the dynamical behaviors of a bubble in a time-periodic electric field by using Poincaré maps. Let us begin with the effect of forcing amplitude for a fixed forcing frequency that is nearly resonant ($\omega=2.348$ while $\omega_n=2.398$). In Fig. 11, the Poincaré map for $\varepsilon=0.05$ is given. By comparing Figs. 8 and 11, we can immediately see that the regular region for bounded bubble motion shrinks in size significantly. Physically this means that the probability of escape to rapid growth increases as the amplitude increases, if the initial condition is distributed uniformly in the phase plane.

As mentioned previously, the dynamics depends heavily on the initial condition even for the fixed parameters such as the average Weber number, amplitude, frequency, and the damping coefficient. To see this

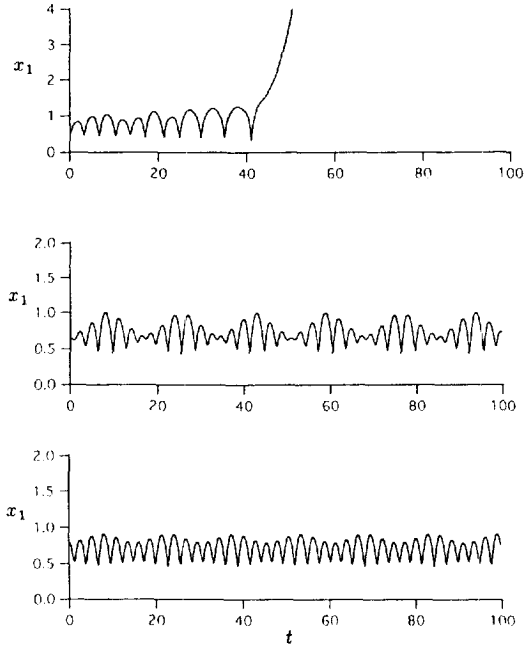

Fig. 12. The effect of initial conditions on the bubble dynamics for the case of nearly resonant forcing ($\omega=2.348$) when $\varepsilon=0.05$, $W_0=0.0168$.

point, we have plotted $x_1(t)$ for various cases of initial conditions in Fig. 12. The initial conditions considered are $[x_1(0), x_2(0)]=(0.5, 0)$, $(0.65, 0)$ and $(0.8, 0)$, and other parameters for Fig. 12 are the same as those for Fig. 11. When $x_1(0)=0.5$, the initial condition is outside the regular region (or equivalently in the homoclinic tangle region) of the Poincaré map in Fig. 11. As discussed earlier, the bubble exhibits random oscillation for a while and eventually escapes to the rapid growth stage. On the other hand, when the initial conditions are in the regular region $[x_1(0)=0.65, 0.8]$, bubble shows two-timing oscillation as we can see in Fig. 12. From Figs. 11 and 12, we can see again that the size of the regular region can serve as a measure for the effectiveness of time-periodic forcing to get rapid growth of a bubble.

As discussed in the subsection for regular dynamics, the bubble dynamics in time-periodic electric field depends strongly on the forcing frequency. Especially that is the case for the size of the regular region in the Poincaré map. To see this point, the Poincaré map for the case of frequency $\omega=7.05$ is given in Fig. 13. By comparing Fig. 13 with Fig. 11, we can see that the regular region for the bounded oscillation is much larger for the case of $\omega=7.05$ than the case of $\omega=2.348$, which is a nearly resonant value. In other

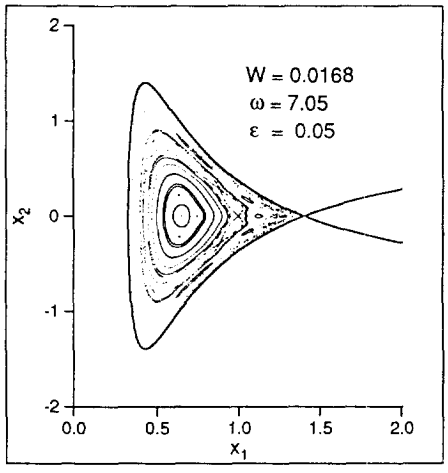

Fig. 13. The Poincare map for the case of $\varepsilon=0.05$, $W_0=0.0168$ when $\omega=7.05$.

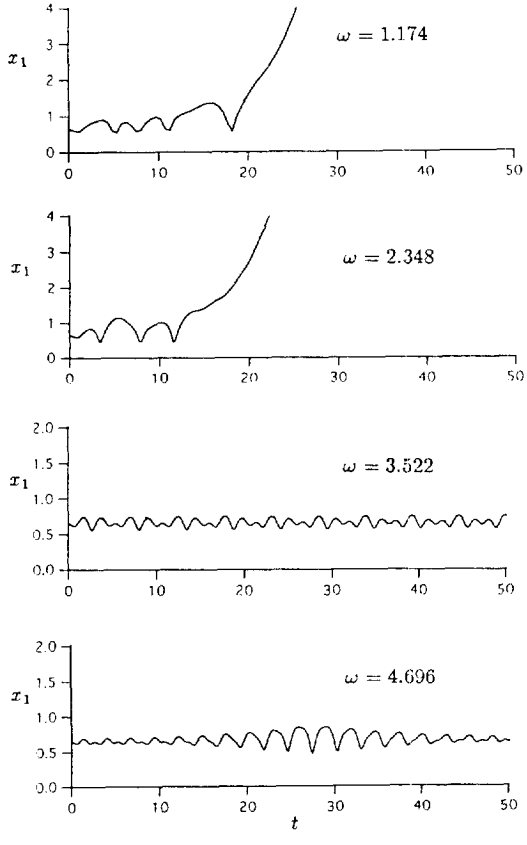

Fig. 14. The effect of forcing frequency on the bubble dynamics for the case of $\varepsilon=0.1$, $W_0=0.0168$, $1/Re=0$, and initial condition $x_1(0)=0.65$.

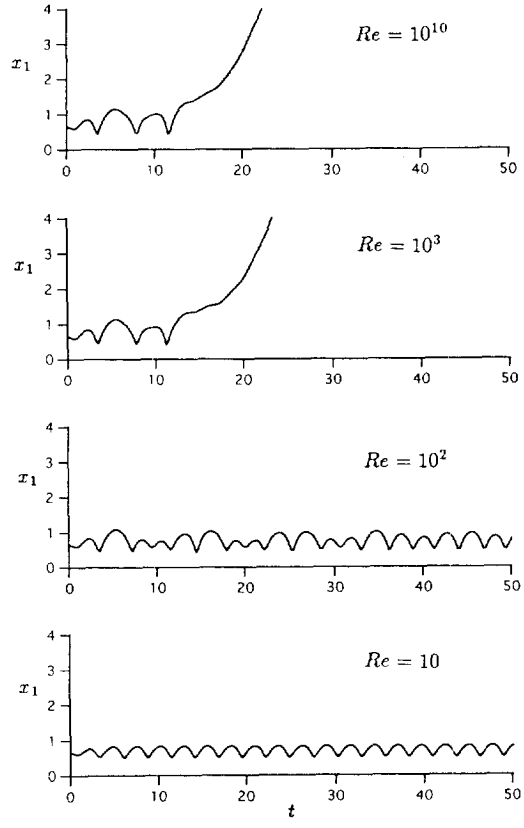

Fig. 15. The effect of viscous damping on the bubble dynamics for the nearly resonant case ($\omega=2.348$) when $\varepsilon=0.1$, $W_0=0.0168$, and initial condition $x_1(0)=0.65$.

words, the probability of escape to the rapid growth stage is much higher in the case of $\omega=2.348$. In order to see the effect of forcing frequency more clearly, a bubble is excited with various frequencies starting from the rest state at equilibrium. In Fig. 14, several plots of $x_1(t)$ are shown for various forcing frequencies with fixed parameters of $W_0=0.0168$, $\varepsilon=0.1$, $1/Re=0$, and $[x_1(0), x_2(0)]=(0.65, 0)$. From Fig. 14, we can see that there exists an optimum value of forcing frequency, in the sense of increasing the probability of escape from the bounded oscillation. The optimum frequency is found to be the value that is slightly lower than the intrinsic resonant frequency.

The effect of viscous damping on the bubble dynamics is also considered. In Fig. 15, the bubble dynamics for different levels of viscous damping are shown. The parameters for Fig. 15 are $W_0=0.0168$, $\varepsilon=0.1$, $\omega=2.348$, and $[x_1(0), x_2(0)]=(0.65, 0)$. As we can see in Fig. 15, we could get the escape to the rapid growth

stage if viscous damping is not sufficiently strong (see the cases of $Re=10^{10}$ and 10^3). However, as the viscous damping is increased further, the bubble dynamics is soon attracted to the steady oscillation as we can see in the cases for $Re=10^2$ and 10.

Thus far, we have considered the effects of time-periodic forcing by an electric field when the pressure difference is fixed. However, if we remember the equivalence of the effects of pressure and electric fields, the results in this section can be easily transformed to the results for the time-periodic forcing by a pressure field without an electric field. As mentioned earlier, if the characteristic length scale in this problem is smaller than $O(10^{-3})$ cm, then the intrinsic oscillation frequency is certainly in the ultrasonic wave frequency range. Thus, the ultrasonic wave can promote the cavitation phenomena as already adopted in many applications. However, in some cases, application of ultrasonic wave may not be suitable. In those cases, time-periodic forcing by an electric field, in a form such as $\mathbf{E}_0(t)=\varepsilon\cos\omega t\mathbf{e}_x$, may be used to promote cavitation. For that purpose, finding an optimal frequency is very important to maximize the efficiency of the time-periodic forcing.

CONCLUSION

In the present work, the dynamics of bubble growth in a time-dependent electric field has been investigated via the modified Rayleigh-Plesset equation where the effect of an electric field is added. The effect of an imposed electric field was found to be equivalent to the increase of the ambient pressure by the amount $(3/8)\varepsilon_0 E_0^2\varepsilon_1(2S-1)$. This result agrees with the ealier finding of Marston and Apfel [2].

For a given pressure difference $\Delta P>3.079$, there are two critical Weber numbers W_{c1} and W_{c2} for existence of steady solutions. The number of steady solutions is 0 if $W<W_{c1}$, 2 if $W_{c1}<W<W_{c2}$, and 1 if $W>W_{c2}$. However, if $\Delta P<3.079$, the smaller critical Weber number does not exist.

The effect of steady electric field has been studied via the phase-plane analysis. For a given pressure difference, the electric field has an effect to increase the size of the domain enclosed by the separatrix in the phase-plane, which corresponds to the bounded bubble oscillation. Thus, the steady electric field has an effect of inhibiting cavitation. The intrinsic resonant frequency of oscillation about the stable equilibrium radius is also found to increase as the Weber number increases due to the obvious reason of shrinking size of bubble in an electric field.

The effects of a time-periodic electric field have been studied by using two methods of analysis; two-timing perturbation analysis for the regular dynamics near the stable steady solution and the Poincaré map analysis for the global dynamics. The two-timing analysis revealed that an $O(\varepsilon^{1/3})$ response in the oscillation of bubble radius can be obtained from an $O(\varepsilon)$ resonant time-periodic forcing in the neighborhood of a stable steady solution. The same behavior has been found in the similar problems of bubble or drop dynamics.

The Poincaré map analysis showed that a bubble may escape from the trajectories of bounded oscillation, which would be taken under steady electric field, to rapid growth when the bubble is subject to a time-periodic forcing. Thus, the time-periodic forcing has an effect to reduce the size of the domain of the bounded oscillation in the phase plane. The Poincaré map analysis also showed that the probability of escape to rapid growth can be maximized by choosing an optimal frequency for a fixed amplitude in the time periodic forcing. The optimal frequency was found to be the value that is slightly lower than the intrinsic resonant frequency for small amplitude oscillation in a steady electric field. The significance of this finding is that a time-periodic electric field may be used to promote cavitation while the steady electric field has an effect of inhibiting cavitation. Thus, an electric field may be used for both inhibiting and promoting cavitation depending on the purposes.

Finally, a comment should be given to the possible immediate extensions to the present work. In the present work, we have neglected the effect of bubble deformation that results from the non-uniformity of the normal stress over the surface produced by an electric field. The problem of deformation with constant bubble volume can be touched by various methods such as the domain perturbation method and the method of spheroidal approximation. The analysis on the combined effects of the dynamic growth and deformation of a bubble subject to an electric field may be the next challenge to the present work.

ACKNOWLEDGEMENT

This work was supported by the grant from the Korea Science and Engineering Foundation via the Advanced Fluids Engineering Research Center at the Pohang Institute of Science and Technology.

REFERENCES

1. Suslick, K. S.: *Scientific American*, February, 62

(1989).
2. Marston, P. L. and Apfel, R. E.: *Phys. Letters,* **60A**, 225 (1977).
3. Plesset, M. S. and Prosperetti, A.: *Ann. Rev. Fluid Mech.,* **9**, 145 (1977).
4. Rayleigh, L. (J. W. Strutt): *Phil. Magazine(Series 6),* **34**, 94 (1917).
5. Chang, H.-C. and Chen, L.-H.: *Phys. Fluids,* **29**, 3530 (1986).
6. Szeri, A. J. and Leal, L. G.: *Phys. Fluids A,* **3**, 551 (1991).
7. Kang, I. S. and Leal, L. G.: *J. Fluid Mech.,* **218**, 41 (1990).
8. Melcher, J. R. and Taylor, G. I.: *Ann. Rev. Fluid Mech.,* **1**, 111 (1969).
9. Nafeh, M. H. and Brussel, M. K.: "Electricity and Magnetism", John Wiley, New York, NY (1985).
10. Leal, L. G.: "Laminar Flow and Convective Transport Processes-Scaling Principles and Asymptotic Analysis", Butterworth-Heinemann, Boston, MA (1992).
11. Guckenheimer, J. and Holmes, P. J.: "Nonlinear Oscillations, Dynamical Systems, and Bifurcations of Vector Fields", Appl. Math. Sci. Vol. 42. Springer-Verlag, New York, NY (1983).
12. Kang, I. S.: Dynamics of a Conducting Drop in a Time-Periodic Electric Field, *J. Fluid Mech.,* To appear (1993).
13. Nafeh, A. H. and Mook, D. T.: "Nonlinear Oscillations", Wiley-Interscience, New York, NY (1979).
14. Wiggins, S.: "Global Bifurcations and Chaos-Analytical Methods", Appl. Math. Sci. Vol. 73. Springer-Verlag, New York, NY (1988).